

## The evaluation and application of an urban land cover map with image data fusion and laboratory measurements

LÁSZLÓ MUCSI<sup>1</sup>, CSILLA MARIANN LISKA<sup>1</sup>, LÁSZLÓ HENITS<sup>1</sup>, ZALÁN TOBAK<sup>1</sup>,  
BÁLINT CSENDES<sup>1</sup> and LÁSZLÓ NAGY<sup>2</sup>

### Abstract

High spatial and spectral resolution aerial images make it possible to develop detailed and large-scale (about 1:5,000) urban land cover maps. The main objectives of this study are (1) to evaluate the correlation between laboratory and hyperspectral image spectra to select proper bands and training samples for classification; (2) to develop a classification process to combine the spectral and spatial information of multispectral and hyperspectral images and make an urban land cover map for the study area in Szeged, Hungary; and (3) to examine the effect of different roof types on the modification of surface temperature. Reference materials were collected from the training area and their spectral characteristics were measured by a laboratory spectrometer. The hyperspectral image and laboratory spectral data between 500–800 nm showed a very strong correlation, the correlation coefficient was 0.99. The urban land cover map was produced by the combination of segmentation procedure and Spectral Angle Mapper (SAM) method using the spatial information derived from multispectral image and the spectral information of the hyperspectral image. Eight land cover classes were identified as impervious surfaces (asphalt, 4 types of tiled roof), water, and green vegetation. The overall accuracy of urban land cover map was 87.9 per cent. According to the results, an accurate large-scale urban land cover map can be generated from the fusion of multispectral and hyperspectral images. We presented that certain roof types have significant effect on surface temperature, which is strongly connected to the urban heat island phenomenon, and influences population health.

**Keywords:** urban remote sensing, hyperspectral image, spectral library, surface temperature, land cover classes

### Introduction

The object of geography is to study the dynamically changing relationship between people and their environment in space and time. Cities are key factors in this relational system since 54 per cent of the Earth's population (World Urbanization Prospects, 2014) lives in urban areas. Increasing urbanization generates the dynamic transformation of land cover (LC) and land use (LU) types. The population concentrated in a small area extremely stresses its surrounding environment (MUCSI, L. *et al.* 2008). Increasing energy consumption, heat emission, traffic and waste generation of

cities are important factors at global level, and studying their environment-modifying effect is necessary (SMALL, C. 2003).

The mapping of changing urban land cover, especially the continuously increasing built-up density, is important both on local and global scale. The spatial pattern and intensity of urban heat island (UHI) is strongly connected to the density of impervious surfaces (GÁL, T. *et al.* 2016; HERBEL, I. *et al.* 2016; HENITS, L. *et al.* 2017). The primary aim of this study is to create an accurate land cover map based on the combination of multi- and hyperspectral images, field observations, and laboratory measurements. Imaging spectrom-

<sup>1</sup>Department of Physical Geography and Geoinformatics, University of Szeged, H-6722 Szeged, Egyetem u. 2. E-mail: mucusi@geo.u-szeged.hu (Correspondent author).

<sup>2</sup>Department of Medical Physics and Informatics, University of Szeged, H-6722 Szeged, Egyetem u. 2.

etry has been used for more than 30 years in numerous researches, and has gone through considerable methodical development. By the improvement of technology, these systems (AISA, DAIS, HyMap) are able to cover the electromagnetic spectrum in the range of 400–2,500 nm and in the spectral resolution of 1–10 nm (PLAZA, A. *et al.* 2009). Several studies focused on the mapping of minerals (KRUSE, F.A. 2012) and soil surfaces (LAGACHERIE, P. *et al.* 2008), studying water depth and quality (JAY, S. and GUILLAUME, M. 2014), snow, ice, and tree species (GOETZ, A.F.H. 2009) in the last fifteen years. As for urban applications, for example, the mapping of asbestos-containing roofs, BASSANI, C. *et al.* (2007) and SZABÓ, Sz. *et al.* (2014) should be mentioned. SEGL, K. *et al.* (2003) made statements about the separation of different artificial materials by using laboratory and field measurements. They highlighted that the application of hyperspectral images in contrast with time-consuming field validation is promising for ecological urban planning. However, a relatively small number of spectral libraries are available for urban land cover (BASSANI, C. *et al.* 2007) and the commonly used materials have different spectral characteristics in different regions.

The derivation of spectral curves can be implemented by different methods: they can be established by using the mean reflectance curve of training samples extracted from hyperspectral images, or by field or laboratory measurements (VAN DER MEER, F. *et al.* 2001). As outer physical effects influence aerial survey, the spectrum is slightly different from the spectrum obtained in laboratory circumstances (HEIDEN, U. *et al.* 2007). The settings of the measurements are device specific and depend on the demands of the users (JUNG, A. *et al.* 2012). The laboratory measurements can be applied in the processing of images acquired by different sensors at different time. Because roof angles, illumination effects, shadows and various land cover make the selection of training samples difficult and subjective in the image, we collected laboratory spectra from the study area. Furthermore, the analysis of spectra is necessary to decrease the number

of bands used in the classification procedure, which makes the method capable to apply for bigger city parts. Only the necessary bands or band ranges should be applied (HEROLD, M. and ROBERTS, D.A. 2010; WU, B. *et al.* 2013).

In urban studies the objects in the available hyperspectral aerial image are not easily separable, additional information (high resolution multispectral aerial photo) is needed to define the geometry of objects. Numerous researches were performed data fusion using multispectral data with radar (CHEN, C.M. *et al.* 2003), with Light Detection and Ranging (LIDAR: ALONZO, M. *et al.* 2014), with population census data (JIN, H. and MOUNTRAKIS, G. 2013), and hyperspectral images (GEVAERT, C.M. *et al.* 2014). Our solution is a consecutive segmentation and Spectral Angle Mapper Classification with the combined use of aerial photos (both multi- and hyperspectral) and laboratory measurements.

Segmentation is a well-known solution to derive the borders of certain objects from high resolution images. Object Based Image Analysis (OBIA) was used previously to map forests (CHUBEY, M.S. *et al.* 2006), natural catastrophes (effects of an earthquake: GUSELLA, L. *et al.* 2005) and cities as well (CHEN, Y. *et al.* 2007). It has been established that under appropriate conditions OBIA could be more accurate than pixel-based methods (AL KHUDAIRY, D.H. *et al.* 2005). The OBIA method emphasizes the spatial relation between neighbouring pixels. As a result, pixels being closer in space are more likely to be classified into the same class (BLASCHKE, T. 2010). It should be mentioned that perfect parameters cannot be defined for segmentation. RÄSÄNEN, A. *et al.* (2013) tested more than 200 segmentation results using different input parameters. They assumed that the best result should be determined by the suitability of the application. The segmentation method was supplemented by Spectral Angle Mapper (SAM), which is the most appropriate method for the application of laboratory measurements in the classification since it allows the comparison of two spectra (KRUSE, F.A. *et al.* 1993).

Numerous studies have been carried out to investigate the relationship between land cover and surface temperature. Most of the researchers used low and medium resolution images, e.g. Landsat and MODIS images (ZHOU, W. 2014). Only a few studies applied high resolution thermal imagery for this purpose (BITELLI, G. *et al.* 2015). Previously, for example ROMAN, K.K. *et al.* (2016) described the temperature modification effects of roofs. Since our goal was to make recommendations for the mitigation of the effects of urbanization, we used a thermal aerial photo and our land cover map to analyse the differences between temperature values of the land cover types.

The main objectives of our study were (1) to evaluate the correlation between laboratory and the hyperspectral image spectra to predict the value of laboratory measurements in the classification procedure (dimensionality reduction, training sample selection); (2) to use a multispectral and a hyperspectral image to perform an accurate land-cover classification using the spectral information of hyperspectral and the spatial information of multispectral image; and (3) to analyse the land surface temperature (LST) of different land cover classes.

### Study area

Szeged is the third largest city in Hungary (165,000 inhabitants – Hungarian Central Statistical Office, 2016), and the administrative area of city is 281 km<sup>2</sup>. 95 per cent of the city buildings were destroyed by the flood in 1879, therefore a new structure with boulevards and avenues was built in Szeged (LECHNER, L. 1891). The reconstruction was carried out by using a complex urban planning design based on the work of Lajos LECHNER. This radio-concentric structure of the city has remained unchanged in the last 135 years.

The built-up density of Szeged varied from densely built-up areas (City Centre) through suburban areas to housing estates with blocks of flats and industrial areas. Green areas (forests on the riverbanks) and parks are located among the built-up areas (Mucsi, L. 1996).

In our study, a representative part of this functional unit was selected, which can also be found in other small- and middle-sized Hungarian towns.

In the last 130 years, the characteristics of buildings have significantly changed. Original buildings (houses with the sun-beam motif) can only be found in some cases. Today newly-built detached houses and condominiums are located on most of the lots, and the density of built-up areas has significantly increased. Two blocks of houses, which proved to be appropriate for land cover mapping, were chosen for our study. During field survey and sampling of reference data we found that the selected blocks represented the suburban-like built-up density well (*Figure 1*).

### Data

#### *Hyperspectral aerial surveys*

Hyperspectral aerial surveys were carried out several times using an AISA DUAL hyperspectral instrument (359 spectral bands in the range of 400–2,500 nm, and in 2.3 and 5.8 nm bandwidths, *Table 1*). The chosen hyperspectral image was acquired in September, 2010 with a spatial resolution of 1.5 m. Pixel values were converted to reflectance values using radiometric and atmospheric correction procedures (Mucsi, L. *et al.* 2008) using field reflectance measurements at the time of image acquisition.

#### *Multispectral aerial image*

In addition, a high spatial resolution (< 1 m) natural-colour aerial photo (*Table 1*) was used to improve the classification results because it has higher spatial resolution, and it provides more detailed object border than the hyperspectral image. The image was acquired within the framework of the national aerial survey in August, 2011, and it has a spatial resolution of 0.4 m.

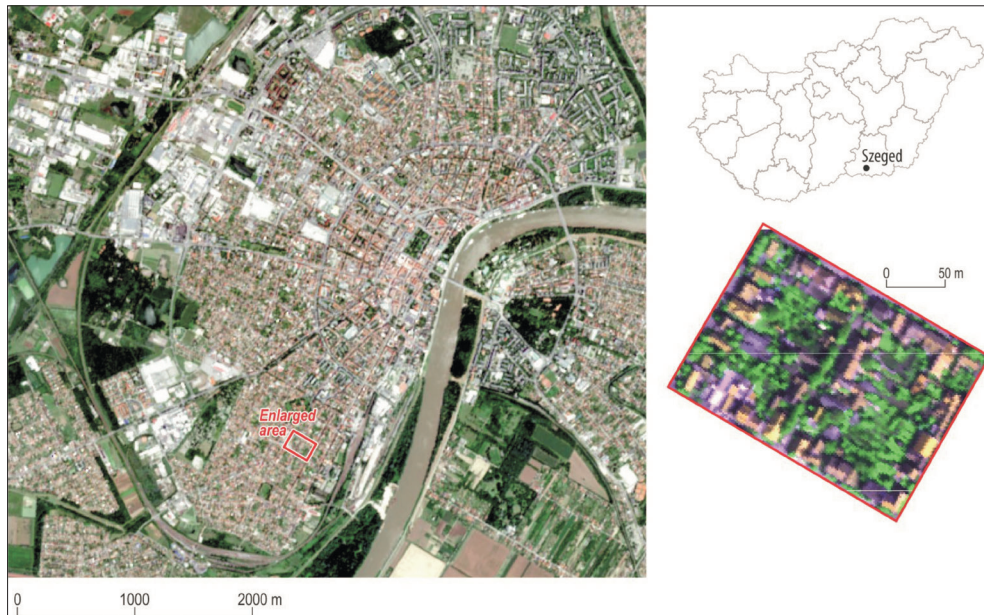


Fig. 1. Study area

### Laboratory measurements

Land cover samples were collected for the laboratory measurements during field survey. The laboratory measurements were performed by an Avantes DH2000 spectrometer at the Department of Medical Physics and Informatics, University of Szeged (Figure 2, Table 1). The device provides data in two ranges: between 350–850 nm (master) and 530–1,150 nm (slave). The bandwidth of the spectrometer varies between 0.27–0.37 nm and the number

of bands is above 2,000. The reflectance values were calculated as averages of 25 sampling.

### Thermal aerial image

For the environmental application, we used thermal images, which were obtained by the thermal camera of Lower Tisza District Water Directorate (ATIVIZIG) and were acquired on 12 and 14 August 2008 (Table 1). The sensor can record data in the range between

Table 1. Summary of the data used in this study

	Spectral resolution	Spatial resolution	Spectral resolution		
Multispectral aerial image	Autumn, 2011	0.4 m	3 bands (true color)		
Hyperspectral aerial image	September, 2010	1.5 m	359 bands (400–2,500 nm)		
Thermal aerial image	August, 2008	2.5 m	1 band, -40 °C– 500 °C		
Laboratory measurements	2013–2014	–	Master	350–850 nm	>2,000 bands
			Slave	525–1,165 nm	>2,000 bands



Fig. 2. Avantes spectrometer and sampling

-40–500 °C and the image has a spatial resolution of 2.5 m. More information about the calibration was presented by UNGER, J. *et al.* (2010).

## Methods

### *Spectral Libraries: training samples and dimension reduction*

The following main land cover materials were collected for laboratory measurement: red clay roof tiles, asphalt, and vegetation. Other roof types were examined (e.g. purple clay roof, claret concrete tile, plastic tiles) but only the red clay tile is explained in more detail, because this is the most common roof type in the study area.

Firstly, we analysed the proper settings of spectrometer and the correlation between laboratory and hyperspectral image. Measurements of all samples were implemented in the aforementioned two partially overlapping ranges (master and slave). These two ranges provided total reflectance curves

from the visible light to the mid-infrared for each material. The standard deviation of the data was high at the edges of relatively wide ranges. In addition, the bandwidth of these two ranges is different and switching between the channels makes the implementation of the measurements difficult.

The geographic coordinates of the collected samples were recorded during the field surveys. Corresponding image pixels were determined on the geo-corrected hyperspectral image using GPS coordinates. The laboratory reflectance spectra of collected samples and the reflectance values derived from pixel values were compared. We determined the widest possible spectral range in which the correlation between laboratory spectrum and hyperspectral data is the highest.

After that we analysed the correlation between laboratory and image spectra. It is an important step, since the laboratory spectra should be used as training sample for Spectral Angle Mapper Classification, instead of selecting pure pixels in the image. The flowchart of the entire data processing is shown in *Figure 3*.

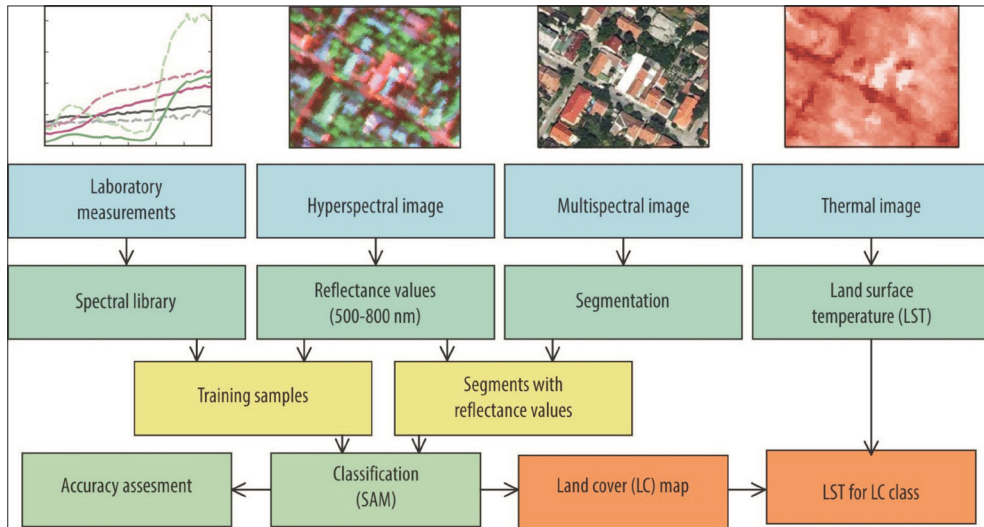


Fig. 3. Flowchart of data processing and analysis

### Segmentation and data fusion

Geometric transformation was performed to align the two images: multi- and hyperspectral images with different spatial resolution. We transformed the natural-colour aerial photo with Ground Control Points (GCPs), and the Root Mean Square Error (RMSE) was lower than 0.5 pixel.

The segmentation module of ERDAS Imagine was applied to the multispectral aerial image. The segmentation parameters were selected with a trial-and-error method approach based on the compute settings parameters function in ERDAS Imagine until satisfactory results were achieved. Edge detection was performed on the multispectral image, and the minimum segment size was set to 25 pixels (4 m<sup>2</sup>). The minimum spectral distance and the variance factor values were modified to extract separate segments. Higher minimum spectral distance value results in the smaller number of segments. When the spectral distance between neighbouring pixels are less than the selected value, pixels are assigned to the same segment. Variance is a very important parameter

because larger variance increases the heterogeneity within the segment. Larger variance reduces the number of segments (ERDAS Field Guide, 2013).

During the data fusion process, the multispectral image was segmented, and average reflectance values derived from the hyperspectral image bands were assigned to each segment separately. As a result the spectral parameters of the hyperspectral image were assigned to the spatial objects of multispectral image (Figure 4). Finally, an image segment containing a lot of pixels has only one average reflectance curve, which makes the classification process faster.

### Classification: Spectral Angle Mapper (SAM)

After the average reflectance curves were computed for each segments, we applied the SAM method to classify segments to the proper class based on the similarity of curves of the segments to laboratory curves. By using this method, pixels can be set in an  $n$ -dimensional space ( $n$  is the number of bands). The algorithm selects those pixels which are

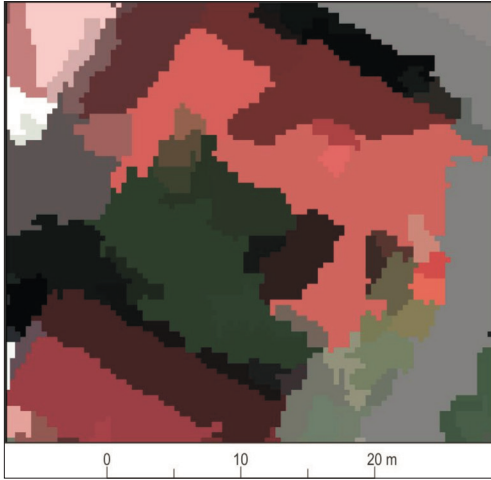


Fig. 4. Result of segmentation and data assignment (RGB: 50,24,12)

within the user-defined deviation range of vectors. A great advantage of this method is that it is only sensitive to the direction of the vector and not to the length of the vector (KRUSE, F.A. et al. 1993).

## Results and discussion

### *Correlation of laboratory measurements and hyperspectral image spectra*

The influence of the distance between the sensor and the material sample was tested at the beginning of laboratory measurements. It was observed that increasing distance increased the deviation in the range of shorter and longer wavelengths. Therefore, we used 2 cm subject distance to measure the reflectance for all samples.

The analysis of the total spectra of master and slave channels showed that high correlation coefficient occurred only in the master channel for clay roof tile and vegetation ( $R=0.98$ ), while this relationship was not so strong ( $R=0.52$ ) for asphalt (Table 2). Significantly smaller values were obtained in the slave channel for each land cover material. The values of the correlation coefficients increased by narrowing the spectral range. High and significant relationship was calculated in the overlapping bands of the master and slave channels between 525–800 nm for each material. Since the reflectance curves of each material were quite similar at 525 nm, we chose the spectral range between 500–800 nm which was a wider range but it gave a slightly lower value for asphalt. In addition, the reflectance value of the vegetation was the lowest in the range between 500–525 nm and at 525 nm it exceeded the reflectance value of red clay roof tiles and asphalt.

The shape of the reflectance curve derived from selected ranges provided important information about the features of the materials. The reflectance curve of red clay roof tile was monotonically increasing in the range between 500–800 nm (Figure 5). As opposed to this, the curve of the asphalt showed a constant value. The characteristics of the vegetation curve were the most distinct. It had a local maximum at 550 nm (there are two minimums at 450–680 nm because of chlorophyll absorption), and the red edge band could be observed at 775 nm after a decrease of the values. Plant species can be differentiated by determining the inflection point of the reflectance curve in this range (VANE, G. and GOETZ, A.F.H. 1988).

Lots of land cover types can be found in the study area, especially the roof types are

Table 2. Correlation between the sample and the corresponding pixel in different spectral ranges

Wavelength (nm)	Master			Slave	
	350–850	500–800	525–800	525–1,165	525–800
Red clay roof tiles	0.987	0.991	0.990	-0.240	0.982
Vegetation	0.983	0.988	0.988	0.642	0.993
Asphalt	0.519	0.857	0.885	0.303	0.950

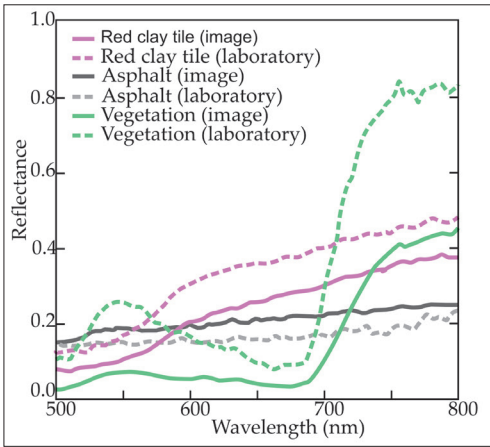


Fig. 5. Reflectance curves of laboratory measurements and derived from the hyperspectral image

heterogeneous. The classes are not separated well in the multispectral images, thus additional information is required for precise classification. Using hyperspectral data, spectral differences between the vegetation and artificial surfaces are so specific that misclassification is mostly expected only between different roof types or other artificial surfaces (e.g. asphalt, greenhouses).

Strong relationship between laboratory and survey spectra is shown in Figure 5. The spectral features determined by laboratory measurements are represented in the hyperspectral image as well, with smaller shifts caused by the aforementioned effects. The local maximum of the vegetation appears at 550 nm both in the image and the laboratory spectra, but the laboratory spectrum is slighter and the inflection point in the red edge range can also be observed. The increasing reflectance values of clay roof tiles and the nearly identical values of asphalt are represented both in laboratory measurements and in hyperspectral image spectra.

After comparing the laboratory and hyperspectral image data, the spectral bands between 500–800 nm were selected for the separation of the main land cover classes. 67 bands can be found in this range on the hyperspectral image.

### Evaluation of built-up map

The urban land cover map was created based on the result of SAM classification (Figure 6) A high spatial resolution aerial photo obtained from the Department of Physical Geography and Geoinformatics, University of Szeged, was used for the accuracy assessment procedure. The natural-colour aerial photo was acquired in March, 2012, and has 0.1 m spatial resolution. We used Google Earth images to classify uncertain reference points because the acquisition date of the reference image differs from the hyperspectral image (due to different vegetation period). We selected a total of 380 points for the study area using stratified random sampling method (Table 3). The accuracy assessment showed that the overall accuracy of the land cover map was high (87.9%). The accuracy value of the least accurate class (asphalt) was 67.2 per cent. Five different roof types, water bodies, roads, and vegetation were separated. Some segments remained unclassified due to the shadow effect and the mixture of different land cover types within the pixels.

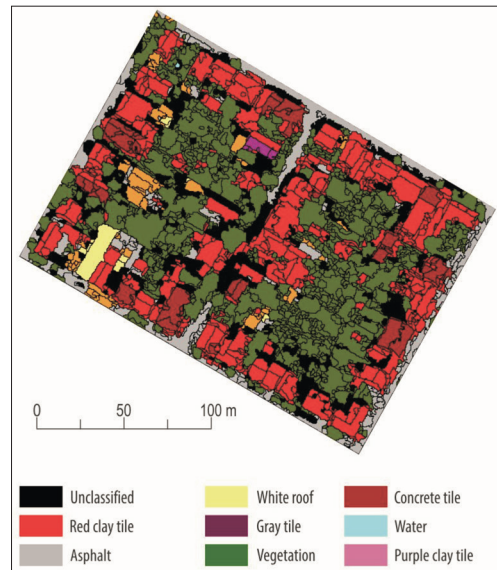


Fig. 6. Land cover map of the study area

Table 3. Stratified random accuracy assessment

Class	Reference points	Classified points	Correctly classified	Producer's accuracy, %	User's accuracy, %
Red clay tile	78	104	72	92.3	69.2
Asphalt	61	45	41	67.2	91.1
White roof	16	14	14	87.5	100.0
Gray tile	18	17	14	77.8	82.4
Vegetation	166	157	154	92.8	98.1
Red concrete tile	27	30	26	96.3	86.7
Water	2	2	2	100.0	100.0
Purple clay tile	12	11	11	91.7	100.0
Sum	380	380	334		

Overall accuracy: 87.9%. Overall Kappa Statistics = 0.84

The vegetation class had high producer's (92.8%) and user's accuracy (98.1%). The producer's and user's accuracy of water was 100 per cent. White roof, red concrete tile, purple clay tile had high producer's accuracies ranging from 87.5 to 96.3 per cent and high user's accuracies ranging from 86.7 to almost 100 per cent. Gray tile had lower producer's (77.8%) and user's accuracy (82.4%). Red clay tile had low user's accuracy (69.2%)

#### Comparison of land cover classes and surface temperature

First, the differences between the temperature of the start and the end point of the flight track were adjusted. Because of the strong correlation between the two images acquired on different dates, we chose the image acquired on 14 August, because this image had higher contrasts. The statistical parameters of surface temperature were calculated for all land cover classes and the results were summarized in a box plot diagram (Figure 7). The figure shows that the surface temperature of roads was remarkably high, and the median value was over 30 °C. The surface temperature of the vegetation class was not as low as we expected. Since the pixels of the canopy partly cover the roads, the vegetation class had higher mean temperature. The difference

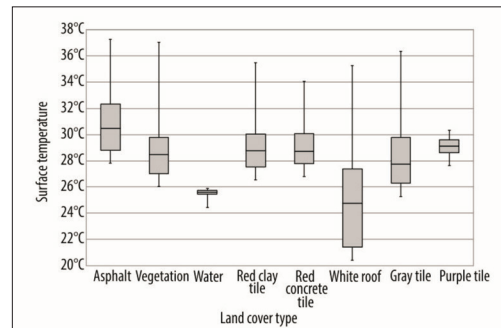


Fig. 7. Comparison of land cover classes and surface temperature on a boxplot diagram

between the temperatures of white roof and other roof types originated from the different material and the function of the building (e.g. the white roof belongs to a cold store). The gray tile had the second lowest mean temperature value. The lower deviation value for water class is originated from the lower number of water pixels in the study area.

#### Conclusions

Hyperspectral data processing is a complex task, which provides unique solution to determine material quality in scientific research. In this study we successfully deter-

mined the extent of built-up area and distinguished 8 land cover types for the study area using laboratory spectra and Spectral Angle Mapper classification method.

Our results provide evidence for the efficiency of laboratory spectra in the selection of training samples based on the high correlation with image spectra. The features of reflectance curves derived from different artificial materials were successfully analysed to determine the most suitable spectral ranges for their separation in feature space. Similar spectral range (580–800 nm) were found with different approach in SZABÓ, Sz. et al. (2014).

In our research two images were used to utilize both the spatial and spectral information of land cover and to improve classification accuracy. Segmentation method was used to gain the geometry of objects from the multispectral image, and Spectral Angle Mapper method was applied for classification based on the divergence of laboratory spectra and hyperspectral data of segments. The methodology proved to be efficient in the image classification of urban area and the overall accuracy was 87.9 per cent. The study of GREIWE, A. and EHLERS, M. (2005) similarly compared single image classification against the joint use of hyperspectral data and high resolution multispectral image. They also used segmentation and SAM scores, and the overall accuracy is significantly increased with the combined use of the RGB image, nDSM (normalized Difference Surface Model) and SAM scores, and the use of SAM scores resulted in almost 20 per cent increase of accuracy. The combination of spectral and spatial classifiers was tested in the mapping of urban land cover using DAIS data in DELL'ACQUA, F. et al. (2004). They stated that higher accuracy can be expected by using spatially connected data, the accuracy of the roof class was 96.4 per cent. Our study also highlighted the importance of spatial scale of urban reflectance, and proved that the high resolution hyperspectral images combined with very high resolution multispectral image can improve urban land cover classification on parcel size. We presented that certain land cover types

have significant effect on surface temperature, which is strongly connected to the urban heat island phenomenon, and influences population health. Most of the citizens cannot afford the green and cool roof types – the advantages are in KOLOKOTSA, D. et al. (2013) –, but can choose from a lot of cheaper roof types, which have preferable temperature properties. Based on our results, the application of certain roof material can be recommended to population which can lead to lower surface temperature locally. Similar temperature modifying effects of roof types were found in ROMAN, K.K. et al. (2016). Further work is needed to consider the effects of the differences in roof angle, texture and age. Consideration should also be given to the mapping of different tree species as the shading capacity of the trees and the modification of microclimate may be different (TAKÁCS, Á. et al. 2016).

The limiting factors of the study were the number of thermal measurements, the small area coverage of hyperspectral data and the narrow range of laboratory measured spectrum. In future research the number of land cover types can be increased by selecting a more heterogeneous study area. The spatial extension of the study can support urban planning programs and provides more detailed information about built-up areas for decision makers.

## REFERENCES

- AL KHUHAIRY, D.H., CARAVAGGI, I. and GLADA, S. 2005. Structural damage assessments from Ikonos data using change detection, object-oriented segmentation, and classification techniques. *Photogrammetric Engineering & Remote Sensing* 71. (7): 825–837.
- ALONZO, M., BOOKHAGEN, B. and ROBERTS, D. A. 2014. Urban tree species mapping using hyperspectral and lidar data fusion. *Remote Sensing of Environment* 148. 70–83.
- BASSANI, C., CAVALLI, R.M., CAVALCANTE, F., CUOMO, V., PALOMBO, A., PESCUCCI, S. and PIGNATTI, S. 2007. Deterioration status of asbestos-cement roofing sheets assessed by analyzing hyperspectral data. *Remote Sensing of Environment* 109. (3): 361–378.
- BITELLI, G., CONTE, P., CSOKNYAI, T., FRANCI, F., GIRELLI, V.A. and MANDANICI, E. 2015. Aerial

- Thermography for Energetic Modelling of Cities. *Remote Sensing* 7. (2): 2152–2170.
- BLASCHKE, T. 2010. Object based image analysis for remote sensing. *ISPRS Journal of Photogrammetry and Remote Sensing* 65. 2–16.
- CHEN, C.M., HEPNER, G.F. and FORSTER, R.R. 2003. Fusion of Hyperspectral and radar data using the HIS transformation to enhance urban surface features. *ISPRS Journal of Photogrammetry and Remote Sensing* 58. (1–2): 19–30.
- CHEN, Y., SHI, P., FUNG, T., WANG, J. and LI, Y. 2007. Object-oriented classification for urban land cover mapping with ASTER imagery. *International Journal of Remote Sensing* 28. (20): 4645–4651.
- CHUBEY, M.S., FRANKLIN, S.E. and WULDER, M.A. 2006. Object-based analysis of IKONOS-2 imagery for extraction of forest inventory parameters. *Photogrammetric Engineering & Remote Sensing* 72. (4): 383–394.
- DELL'ACQUA, F., GAMBA, P., FERRARI, A. PALMASON, J.A., BENEDIKTSSON, J.A. and ARNASON, K. 2004. Exploiting spectral and spatial information in hyperspectral urban data with high resolution. *IEEE Geoscience and Remote Sensing Letters* 1. (4): 322–326.
- ERDAS Field Guide 2013. ERDAS, Inc. Norcross – GA 30092-2500 USA 812. URL: <http://e2b.erdas.com/products/ERDAS-IMAGINE/ProductLiterature.aspx>
- GÁL, T., SKARBIT, N. and UNGER, J. 2016. Urban heat island patterns and their dynamics based on an urban climate measurement network. *Hungarian Geographical Bulletin* 65. (2): 105–116.
- GEVAERT, C.M., TANG, J., GARCIA-HARO, F.J., SUOMALAINEN, J.M. and KOOISTRA, L. 2014. Combining hyperspectral UAV and multispectral Formosat-2 imagery for precision agriculture applications. In *Proceedings WHISPERS 6<sup>th</sup> Workshop on Hyperspectral Image and Signal Processing: Evolution in remote sensing*. Lausanne, Switzerland, 24–26. 06. 2014.
- GOETZ, A.F.H. 2009. Three decades of hyperspectral remote sensing of the Earth: A personal view. *Remote Sensing of Environment* 113. (Supplement 1), 5–16.
- GREIWE, A. and EHLERS, M. 2005. Combined analysis of hyperspectral and high resolution image data in an object oriented classification approach. In *Proceedings of 3<sup>rd</sup> International Symposium on Remote Sensing and Data Fusion over Urban Areas*. Citeseer.
- GUSELLA, L., ADAMS, B.J., BITELLI, G., HUYCK, C.K., EERI, M. and MOGNOL, A. 2005. Object-oriented image understanding and post-earthquake damage assessment for the 2003 Bam, Iran, Earthquake. *Earthquake Spectra* 21. (1): 225–238.
- HEIDEN, U., SEGL, K., ROESSNER, S. and KAUFMANN, H. 2007. Determination of robust spectral features for identification of urban surface materials in hyperspectral remote sensing data. *Remote Sensing of Environment* 111. (4): 537–552.
- HENITS, L., MUCSI, L. and LISKA, C. M. 2017. Monitoring the changes in impervious surface ratio and urban heat island intensity between 1987 and 2011 in Szeged, Hungary. *Environmental Monitoring and Assessment* 189. (2): 1–13.
- HERBEL, I., CROITORU, A.E., RUS, I., HARPA, G.V. and CIUPERTEA, A.F. 2016. Detection of atmospheric urban heat island through direct measurements in Cluj-Napoca city, Romania. *Hungarian Geographical Bulletin* 65. (2): 117–128.
- HEROLD, M. and ROBERTS, D.A. 2010. The Spectral Dimension in Urban Remote Sensing. In *Remote Sensing of Urban and Suburban Areas, Remote Sensing and Digital Image Processing*. Eds.: RASHED, T. and JÜRGENS, C., Dordrecht, Springer, 47–66.
- JAY, S. and GUILLAUME, M. 2014. A novel maximum likelihood based method for mapping depth and water quality from hyperspectral remote-sensing data. *Remote Sensing of Environment* 147, 121–132.
- JIN, H. and MOUNTRAKIS, G. 2013. Integration of urban growth modelling products with image-based urban change analysis. *International Journal of Remote Sensing* 34. (15): 5468–5486.
- JUNG, A., GÖTZE, C. and GLÄSSER, C. 2012. Overview of experimental setups in spectroscopic laboratory measurements – the SpecTour Project. *Photogrammetrie-Fernerkundung-Geoinformation* 4. 433–442.
- KOLOKOTSA, D., SANTAMOURIS, M., ZEREFOS, S.C. 2013. Green and cool roofs' urban heat island mitigation potential in European climates for office buildings under free floating conditions *Solar Energy* 95. 118–130.
- KRUSE, F.A. 2012. Mapping surface mineralogy using imaging spectrometry. *Geomorphology* 137. 41–56.
- KRUSE, F.A., LEFKOFF, A.B., BOARDMAN, J.W., HEIDEBRECHT, K.B., SHAPIRO, A.T., BARLOON, P.J. and GOETZ, A.F.H. 1993. The Spectral Image Processing System (SIPS) Interactive Visualization and Analysis of Imaging Spectrometer Data. *Remote Sensing of Environment* 44. 145–163.
- LAGACHERIE, P., BARET, F., FERET, J.B., NETTO, J. M. and ROBBEZ-MASSON, J.M. 2008. Estimation of soil clay and calcium carbonate using laboratory, field and airborne hyperspectral measurements. *Remote Sensing of Environment* 112. (3): 825–835.
- LECHNER, L. 1891. Szeged újjá építése. (Rebuilding Szeged) Reprint edition in 2000 (in Hungarian).
- MUCSI, L. 1996. Urban land use investigation with GIS and RS methods. *Acta Universitatis Szegediensis Acta Geographica* 25. 111–119.
- MUCSI, L., TOBAK, Z., VAN LEEUWEN, B., SZATMÁRI, J. and KOVÁCS, F. 2008. Analyses of spatial and temporal changes of the urban environment using multi- and hyperspectral data. In *Remote Sensing – New Challenges of High Resolution: proceedings of the EARSeL Joint Workshop*. Ed.: JÜRGENS, C., Bochum, Geographischen Instituts der Ruhr-Universität Bochum, 275–286.

- PLAZA, A., BENEDIKTSSON, J.A., BOARDMAN, J.W., BRAZILE, J., BRUZZONE, L., CAMPS-VALLS, G., CHANUSSOT, J., FAUVEL, M., GAMBA, P., GUALTIERI, A., MARCONCINI, M., TILTON, J.C. and TRIANNI, G. 2009. Recent advances in techniques for hyperspectral image processing. *Remote Sensing of Environment* 113. 110–122.
- RÄSÄNEN, A., RUSANEN, A., KUITUNEN, M. and LENSU, A. 2013. What makes segmentation good? A case study in boreal forest habitat mapping. *International Journal of Remote Sensing* 34. 8603–8627.
- ROMAN, K.K., O'BRIEN, T., ALVEY, J.B., WOO, O.J. 2016. Simulating the effects of cool roof and PCM (phase change materials) based roof to mitigate UHI (urban heat island) in prominent US cities. *Energy* 96. 103–117.
- SEGL, K., ROESSNER, S., HEIDEN, U. and KAUFMANN, H. 2003. Fusion of spectral and shape features for identification of urban surface cover types using reflective and thermal hyperspectral data. *ISPRS Journal of Photogrammetry and Remote Sensing* 58. (1–2): 99–112.
- SMALL, C. 2003. High spatial resolution spectral mixture analysis of urban reflectance. *Remote Sensing of Environment* 88. (1–2): 170–186.
- SZABÓ, SZ., BURAI, P., KOVÁCS, Z., SZABÓ, GY., KERÉNYI, A., FAZEKAS, I., PALÁDI, M., BUDAY, T. and SZABÓ, G. 2014. Testing of algorithms for the identification of asbestos roofing based on hyperspectral data. *Environmental Engineering and Management Journal* 143. (11): 2875–2880.
- TAKÁCS, Á., KOVÁCS, A., KISS, M., GULYÁS, Á., and KÁNTOR, N. 2016. Study on the transmissivity characteristics of urban trees in Szeged, Hungary. *Hungarian Geographical Bulletin* 65. (2): 155–167.
- UNGER, J., GÁL, T., RAKONCZAI, J., MUCSI, L., SZATMÁRI, J., TOBAK, Z., VAN LEEUWEN, B. and FIALA, K. 2010. Modeling of the urban heat island pattern based on the relationship between surface and air temperatures. *Időjárás / Quarterly Journal of the Hungarian Meteorological Service* 14. 287–302.
- VAN DER MEER, F., DE JONG, S.M. and BAKKER, W. 2001. Imaging Spectrometry: Basic analytical techniques. In *Imaging Spectrometry: Basic Principles and Prospective Applications*. Eds.: VAN DER MEER, F., FREEK, D. and JONG, S.M., Dordrecht, Kluwer Academic Publishers, 17–61.
- VANE, G. and GOETZ, A.F.H. 1988. Terrestrial imaging spectroscopy. *Remote Sensing of Environment* 24. 1–29.
- World Urbanization Prospects. The 2014 Revision, Highlights, (ST/ESA/SER.A/352) United Nations, Department of Economic and Social Affairs, Population Division. 2014, 27.
- WU, B., CHEN, C., KECHADI, T.M. and SUN, L. 2013. A comparative evaluation of filter-based feature selection methods for hyper-spectral band selection. *International Journal of Remote Sensing* 34. (22): 7974–7990.
- ZHOU, W., QIAN, Q., LI, X., LI, W. and HAN, L. 2014. Relationships between land cover and the surface urban heat island: seasonal variability and effects of spatial and thematic resolution of land cover data on predicting land surface temperatures. *Landscape Ecology* 29. (1): 153–167.